Study of OFDM Precoded Filter-Bank Waveforms

David Demmer, Rostom Zakaria, Robin Gerzaguet, Jean-Baptiste Doré, Didier Le Ruyet

▶ **To cite this version:**

David Demmer, Rostom Zakaria, Robin Gerzaguet, Jean-Baptiste Doré, Didier Le Ruyet. Study of OFDM Precoded Filter-Bank Waveforms. IEEE Transactions on Wireless Communications, 2019, 18 (6), pp.2889-2902. 10.1109/TWC.2018.2886886 . hal-02470207

HAL Id: hal-02470207
https://cnam.hal.science/hal-02470207

Submitted on 7 Feb 2020

HAL is a multi-disciplinary open access archive for the deposit and dissemination of scientific research documents, whether they are published or not. The documents may come from teaching and research institutions in France or abroad, or from public or private research centers.

L'archive ouverte pluridisciplinaire **HAL**, est destinée au dépôt et à la diffusion de documents scientifiques de niveau recherche, publiés ou non, émanant des établissements d'enseignement et de recherche français ou étrangers, des laboratoires publics ou privés.

Study of OFDM Precoded Filter-Bank Waveforms

David Demmer*†, Rostom Zakaria†, Robin Gerzaguet‡, Jean-Baptiste Doré*, Didier Le Ruyet†
*CEA-Leti, Grenoble, France, {david.demmer, jean-baptiste.dore}@cea.fr
†Conservatoire National des Arts et Métiers, Paris, France, {rostom.zakaria, didier.le_ruyet}@cnam.fr
‡Univ Rennes 1, CNRS, IRISA, France, robin.gerzaguet@irisa.fr

***Abstract*—Forthcoming wireless systems will have to cope with a heterogeneous and dense traffic. High demands in terms of bandwidth use efficiency and increased flexibility are therefore required for the related air-interface technology. In this context, Filter-Bank MultiCarrier with Offset QAM (FBMC/OQAM) waveform has been recognized as an enabling technology providing strong assets with a well confined spectrum and enhanced spectral efficiency with respect to Cyclic Prefix Orthogonal Frequency Division Multiplexing (CP-OFDM). Nonetheless, FBMC-OQAM presents a few challenges to overcome: the intrinsic interference must be taken into consideration in the channel estimation processes and multiple antenna schemes design. Those challenges are induced by the reduction of the orthogonality property to the real field.**

In this paper, OFDM precoding/decoding is proposed as an alternative to the OQAM signaling for filter-bank based waveforms. The OFDM precoding makes the waveforms near-complex orthogonal which enables a straightforward adaptation to channel estimation techniques and MIMO scheme design. Two waveforms based on this precoding, namely Fast Fourier Transform FBMC (FFT-FBMC) and Block Filtered OFDM (BF-OFDM), have been proposed. A common framework is proposed to study the two waveforms. The paper also investigates changing the time structure of the transmitted signal by introducing the rate factor parameter. It is shown that intrinsic interference can be greatly reduced at the price of a slight side-lobe increase.

***Index Terms*—FFT-FBMC, BF-OFDM, intrinsic interference rejection, LTE numerology**

I. Introduction

Wireless communications have experienced considerable changes over the past decades. While the cellular system was initially designed for low data-rate Human-to-Human calls, broadband internet access with its huge data consumption on the downlink is now supported with 4G Long Term Evolution (LTE). Cellular networks are now considered to also support Machine-Type-Communications (MTC) [1][2] which highly differ from typical LTE applications. Indeed, they can be sporadic with a long 'idle-state' period and critical communications require low latency transmissions. It pushes the forthcoming wireless technologies to favor superior flexibility and ensure high network availability. It can be done by first relying on appropriate spectrum-sharing techniques but also by facilitating the network access [3].

Cyclic-Prefix Orthogonal Frequency Division Multiplexing (CP-OFDM) has prevailed in many wireless standards for multiple reasons. First, the waveform provides an interesting robustness against multi-path channels thanks to the CP insertion allowing a 1-tap per sub-carrier equalization. Moreover, CP-OFDM can achieve near-Nyquist rate with an efficient bandwidth use. Last but not least, it can be efficiently implemented by means of (Inverse) Fast Fourier Transform (I-FFT) blocks. Nonetheless, CP-OFDM generates significant Out-of-Band (OOB) emissions because of its rectangular pulse shaping. Besides, as the waveform is based on the complex orthogonality condition, it requires a strict synchronization in both time and frequency domains. These drawbacks make CP-OFDM poorly appealing for future wireless technologies which has encouraged the development of alternative solutions.

Filter Bank Multi-Carrier (FBMC) modulation schemes have therefore gained high interest for such applications [4]. Indeed, FBMC waveforms exhibit high side lobe rejection thanks to its sub-carrier wise filtering and provide an efficient hardware implementation as well with the Poly-Phase Networks (PPN) implementation [5][6]. However, such schemes can not ensure both orthogonality and high spectral efficiency simultaneously. One solution is

to relax one of the properties such as for instance the FBMC-OQAM (standing for Offset Quadrature Amplitude Modulations) that only relies on the real orthogonality[4][7].

Those two examples illustrate the complexity of designing a waveform which is dealing with the Balian-Low Theorem (BLT) [8][9]. It states that a trade-off must be established between three properties which are i) being orthogonal ii) being well localized in both time and frequency domains and iii) ensuring maximum density. From a waveform perspective, the orthogonality is the capacity to cancel intrinsic interference (induced by the waveform itself and not by any propagation and/or RF impairments). Then, considered signals are assumed to be limited in time (and thus have perfect time localization). Therefore, the second property defines the spectral confinement of the waveform and its unwanted OOB emissions. When it comes to the waveform density, it is related to the spectral efficiency of the waveform and thus its maximum useful rate. Those three properties are desired but however can't be fully satisfied simultaneously. A first way to deal with BLT is to greatly relax one of the properties to maximize the two others. It is the case of the two aforementioned waveforms. CP-OFDM is built to perfectly satisfy the orthogonality condition and provide high waveform density (efficient bandwidth use and slight symbol density reduction induced by the CP insertion). Consequently, the spectral confinement is relaxed and CP-OFDM emits high OOB emissions. When it comes to FBMC-OQAM, it is designed to provide a selective filtering and a unitary waveform density. It is made possible by reducing the orthogonality condition to the real-field. The signal recovery is nonetheless ensured thanks to a joint OQAM transmission fitted with a specific phase shift and a Nyquist prototype filter[10]–[12]. However, the reduction of the orthogonality property to the real field makes the adaptation to certain state-of-the-art techniques complex. For instance, Maximum Likelihood detection can not easily applied to FBMC-OQAM. An adaptation based on interference estimation and cancellation has been proposed in [13]. When it comes to Alamouti techniques, a pseudo-Alamouti scheme is presented in [14] that requires in CP insertion and a block Alamouti scheme is introduced in [15] which also leads to a spectral efficiency reduction so as to ensure block isolation. Moreover for the latter scheme, the channel should remain static during the block duration which makes this scheme difficult to implement in time varying environment.

This way of dealing with BLT (by relaxing one condition) proves to be not fully compatible with the purpose of future wireless technologies. The idea is therefore to find a better trade-off between the three conditions where none of them is neglected. One solution is to filter a CP-OFDM signal to improve its spectral confinement which gives us a first family of "post-OFDM" waveforms as for instance UF-OFDM [16], f-OFDM [17] or WOLA-OFDM [18]. In this paper, we will rather tend to improve the orthogonality property of a filter-bank based waveform. The idea is to benefit from its inherent good spectral confinement. It has been shown in [19] that fitting FBMC-OQAM with Coded Division Multiple Access (CDMA) can restore the complex orthogonality and thus allows a straightforward application of the Alamouti scheme. Nevertheless, the scheme still relies on an OQAM transmission and it has been observed that only half the filter bank carriers can be used. The idea has been improved in [20] where the orthogonality of a filter-bank is ensured by applying Hadamard codes. However, the latter suffers from high Inter-Symbol Interference (ISI) when moderate/high channel delay spreads are considered. In this paper, we propose an alternative to the aforementioned filter-bank precoding schemes. The proposed precoding scheme still relies on an orthogonal spreading code and can partially restore the complex orthogonality allowing straightforward state-of-the-art transmission techniques reuse. The considered orthogonal base for the precoding is the OFDM. As it is defined in the frequency domain it can avoid overlap between adjacent bands and thus highly improve the orthogonality of a filter-bank. Such precoding does not require an OQAM transmission which, as it will be studied later on, relaxes the filter design constraints and can be efficiently implemented. Two waveforms, namely Fast-Fourier-Transform FBMC (FFT-FBMC) and Block-Filtered OFDM (BF-OFDM), relying on the proposed precoding scheme will be studied in this paper.

The two waveforms has been respectively proposed in [21][22] and [23][24]. Albeit being very similar, the major difference between these two proposals lies on the receiver scheme. The main

contributions of this study are the following ones:

- Proposal of a generic and common mathematical framework for the two waveforms
- Proposal of a generalized description for the two waveforms where a new parameter, the rate factor, is introduced and studying its impact on intrinsic interference rejection
- Adaptation of the proposed waveforms to the LTE numerology with the corresponding filter design
- Evaluation waveform performance in key scenarios and performance comparison with respect to CP-OFDM and FBMC/OQAM.

The remainder of the paper is organized as follows. In Section II, the analytical models of the two waveforms are derived for both waveforms. The newly-introduced rate factor is considered in the system models. The LTE numerology is derived in Section III. Performance evaluation is given in Section IV. The intrinsic interference distribution, spectral confinement, performance over highly selective channel models and asynchronous multi-user uplink scenario will be considered. Finally, the last section draws concluding comments.

LIST OF SYMBOLS

$(f \star g)[n]$ Discrete convolution product between discrete functions f and g expressed in n

$f_{\uparrow N}, f_{\downarrow N}$ Upsampling, downsampling by a factor N

$\lfloor x \rfloor, \lceil x \rceil$ Floor, ceiling operators

II. WAVEFORM PRINCIPLES

A. FFT-FBMC waveform

1) State-of-the-Art Description

The FFT-FBMC transceiver was proposed to overcome the ISI and InterCarrier Interference (ICI) inherent in FBMC/OQAM scheme. Indeed, the FBMC/OQAM signal in a given subcarrier suffers from ISI and interferes with the signals of the adjacent subcarriers [7][12]. The main idea behind the FFT-FBMC scheme lies in considering an alternative precoding to the OQAM scheme to come up with the intrinsic interference induced by the filter-bank. The proposed precoding is performed by means of Discrete Fourier Transforms (DFT) and CP insertion (like an OFDM Transmitter (Tx)) [21][22] and thus the filter-bank is now used to filter at the subband level. The OFDM precoding scheme provides the flexibility to allocate only a part of the subband and therefore to avoid adjacent subband overlapping. At the receiver side, a matched processing is performed.

For the sake of clarity, the FFT-FBMC transmitter is depicted in Fig. 1. Regarding the notations M denotes the number of subbands (*i.e.* filter-bank (FB) carriers) and N the number of subcarriers per subband (*i.e.* size of the IDFT in the precoding stage). The principle of such scheme can be summarized as follows. Blocks of $N/2$ data complex symbols in each subband k go through an N-IFFT. The $N/2$ data symbols are fed into the first and last $N/4$ bins of the N-IFFT. After that, the N-IFFT outputs are extended with a cyclic prefix (CP) of size N_{CP}, and fed into the FB modulator in a given carrier k.

Let $d_{k,l}[p]$ denote the p^{th} input complex symbol transmitted over the l^{th} subcarrier of the k^{th} subband. Therefore the output of the precoding stage at time instant n and for the k^{th} subband, $a_k[n]$ can be written as [22]:

$$\begin{aligned} a_k[n] &= \sum_{l\in\Omega}\sum_{p} d_{k,l}[p]\Pi_{N_e}[n-pN_e]e^{j\frac{2\pi nl}{N}} \\ &= \sum_{l\in\Omega}\left(d_{k,l}[n]_{\uparrow N_e} \star \Pi_{N_e}[n]\right)e^{j\frac{2\pi nl}{N}} \end{aligned} \quad (1)$$

where Π_{N_e} is a rectangular filter of length $N_e = N + N_{\mathrm{CP}}$, and $\Omega \subset \{0, ..., N-1\}$ is the set of the $N/2$ active subcarrier indices. The transmitted signal after filter-bank processing can therefore be expressed as:

$$\begin{aligned} s[m] &= \sum_{n}\sum_{k=0}^{M-1} a_k[n]g[m-nM/2]e^{j\frac{2\pi km}{M}} \\ &= \sum_{k=0}^{M-1}\left(a_k[m]_{\uparrow\frac{M}{2}} \star g[m]\right)e^{j\frac{2\pi km}{M}} \end{aligned} \quad (2)$$

with g the impulse response of the prototype filter. Therefore, by inserting (1) in (2) we obtain:

$$\begin{aligned} s[m] = \sum_{k=0}^{M-1}\sum_{l\in\Omega}\Bigg(\Bigg(\left(d_{k,l}[m]_{\uparrow N_e} \star \Pi_{N_e}[m]\right)e^{j\frac{2\pi ml}{N}}\Bigg)_{\uparrow\frac{M}{2}} \\ \star\, g[m]\Bigg) \times e^{j\frac{2\pi km}{M}} \end{aligned} \quad (3)$$

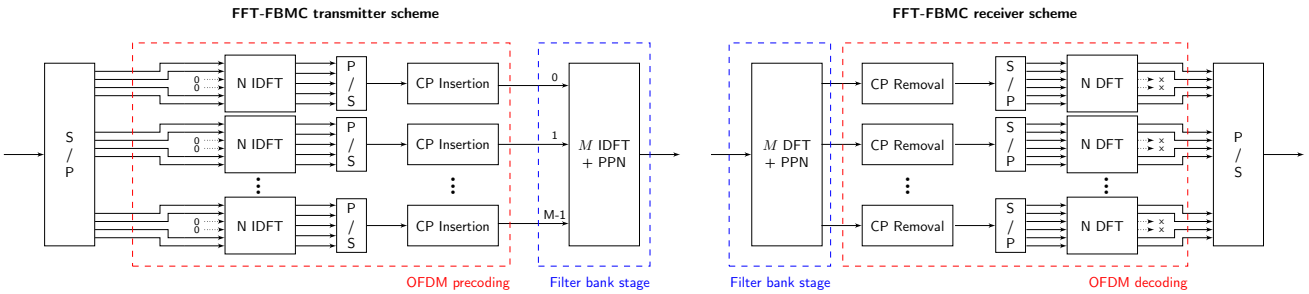

Figure 1. FFT-FBMC transmitter and receiver schemes

$$s[m] = \sum_{k=0}^{M-1} \sum_{l \in \Omega} \Bigg((d_{k,l}[m]_{\uparrow N_e} \star \Pi_{N_e}[m])_{\uparrow \frac{M}{2}} \star g_l[m] \Bigg) e^{j \frac{4\pi m}{MN}(l + \frac{kN}{2})} \quad (4)$$

with $g_l[m] = g[m] e^{-j \frac{4\pi ml}{MN}}$.

The FFT-FBMC receiver scheme is depicted in Figure 1. The received signal is denoted by $y[m]$. For the analytical study, the impact of a channel and the noise are not considered. Indeed, the proposed analytical study focuses on the intrinsic interference rejection and therefore other sources of interferences are not considered in this first section. Thus, $\forall m$ $y[m] = s[m]$. The received signal is processed in a first time by the analysis filter bank. It is assumed that the prototype filter is the same as in the transmitter side. Therefore, the expression of the output of the q^{th}-carrier of the FB at time instant p' can be expressed as in (5). The symbols $z_q[p']$ are then processed by the matched precoding scheme as shown in (6). The CP is discarded and N symbols per block are fed into an N-FFT whose only $N/2$ output symbols $r_{q,l'}[p']$ are kept for detection.

$$z_q[p'] = \left(\left(y[p'] e^{-j \frac{2\pi q p'}{M}} \right) \star g[-p'] \right)_{\downarrow \frac{M}{2}} \quad (5)$$

$$r_{q,l'}[p'] = \left(\left(z_q[p'] e^{-j \frac{2\pi p' l'}{N}} \right) \star \Pi_N[p'] \right)_{\downarrow N_e} \quad (6)$$

2) Generalized Description with a rate of $\frac{1}{\delta M}$

The initial FFT-FBMC scheme presented in the previous paragraph and in [22] is based on the conventional FBMC/OQAM where the narrowband signal rate is $2/M$ (symbols are transmitted every $M/2$ samples) as it has been presented in the previous paragraph and in [22]. In this work, we propose to generalize the description of the scheme where the narrowband rate is set to $\frac{1}{\delta M}$ with δ the rate factor (*i.e.* symbols are transmitted every $M\delta$ symbols). Therefore, the expression of the transmitted signal is generalized by

$$\begin{aligned} s[m] &= \sum_{k=0}^{M-1} \Big(a_k[m]_{\uparrow \delta M} \star g[m] \Big) e^{j \frac{2\pi km}{M}} \\ &= \sum_{k=0}^{M-1} \sum_{l \in \Omega} \Big((d_{k,l}[m]_{\uparrow N_e} \star \Pi_{N_e}[m])_{\uparrow \delta M} \star g_l[m] \Big) \times \\ &\quad e^{j \frac{2\pi m}{\delta MN}(l + \delta kN)} \end{aligned} \quad (7)$$

with $g_l[m] = g[m] e^{-j \frac{2\pi ml}{\delta MN}}$.

Modifying the time structure of the signal have consequences on its spectrum. To determine the subband allocation that prevents adajcent subbands overlap, one can study the frequency response of the transmitted signal. The Power Spectral Density (PSD) expression can be derived by following the procedure given in [25]. By assuming a normalized constellation, the PSD of $(d_{k,l}[m]_{\uparrow N_e} \star \Pi_{N_e}[m])_{\uparrow \delta M}$ is $\left| \frac{\sin(\pi N_e \delta M f)}{\sin(\pi \delta M f)} \right|^2$ and the PSD of $g_l[m]$ is $\left| G\left(f + \frac{l}{\delta MN}\right) \right|^2$. Therefore the PSD expression for a given frequency tone $\{k, l\}$ is given in (8) and its generalized expression is given in (9). Let $D(x) = \frac{\sin(\pi N_e x)}{\sin(\pi x)}$ be the Dirichlet Kernel.

$$\mathcal{S}_{k,l}(f) = \left| G\left(f - \frac{k}{M}\right) \right|^2 |D(\delta M f - l/N - k\delta)|^2 \quad (8)$$

$$\begin{aligned} \mathcal{S}(f) &= \sum_k \sum_{l \in \Omega_k} \mathcal{S}_{k,l}(f) \\ &= \sum_k \left| G\left(f - \frac{k}{M}\right) \right|^2 \sum_{l \in \Omega_k} |D(\delta M f - l/N - k\delta)|^2 \end{aligned} \quad (9)$$

where Ω_k denotes the set of active subcarriers for the k$^{\text{th}}$ FB-carrier.

The analysis of the PSD expression will give us conditions on Ω_k so as to avoid ICI between adjacent subbands. Indeed if the prototype filter g has a null roll-off, there is no frequency overlap between adjacent subbands and therefore the N subcarriers per subband can be used. We assume that g admits a unitary roll-off, *i.e.* $\forall f \notin [\frac{-1}{M}, \frac{1}{M}]$, $G(f) \approx 0$. Hence, there is frequency overlap between adjacent subbands. We may deactivate certain subbands in order to alleviate this issue. But it will be preferred to use all the subbands with half the main lobe width (*i.e* $1/M$). The number of available subcarriers per subband will thus be reduced. This solution eases the resource allocation as the subband allocation is the same of all the subbands. Therefore, the set Ω of available subcarriers in each subband is given by (10).

$$\Omega = \left\{ \left\lfloor \frac{-\delta N}{2} \right\rfloor + 1, ..., \left\lfloor \frac{\delta N}{2} \right\rfloor \right\} \tag{10}$$

As depicted in Figure 2, we may distinguish three cases as presented below.

- $\delta \leq 1/2$: the period $1/(\delta M)$ of $|D(\delta M f - l/N - k\delta)|$ is larger than the total main lobe width of $G(f)$ *i.e.* $2/M$. In the available main lobe width, *i.e.* $1/M$, we can activate at most $N\delta$ subcarriers $l \in \left\{-\frac{N\delta}{2} + 1, ..., \frac{N\delta}{2}\right\}$. It is worth noticing that for this case, overlap with adjacent subbands is completely avoided.
- $1/2 < \delta < 2/3$: the period $1/(\delta M)$ of $|D(\delta M f - l/N - k\delta)|$ is larger than the available main lobe width of $G(f)$ and larger than $3/(2M)$ which corresponds to the distance between the furthest subcarrier and the cut-off frequency of the prototype filter. In the available main lobe width, we can still activate at most $N\delta$ subcarriers $l \in \left\{-\frac{N\delta}{2} + 1, ..., \frac{N\delta}{2}\right\}$. However, limited-energy overlap between adjacent subbands occur.
- $2/3 \leq \delta$: the period of $|D(\delta M f - l/N - k\delta)|$ is smaller than $3/(2M)$. The inter-subband orthognality can not be guaranted because of high-energy overlap between adjacent subbands. This case will not be considered for the rest of the paper.

When it comes to the receiver, the output of the filter bank stage over the q^{th} carrier at time instant

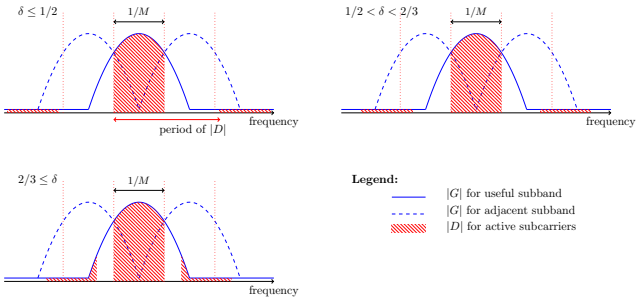

Figure 2. Relation between δ and the inter-subband orthogonality

p', $z_q[p']$, and the received symbol at subcarrier index l' can be expressed as follows:

$$z_q[p'] = \left(\left(y[p'] e^{-j\frac{2\pi q p'}{M}} \right) \star g[-p'] \right)_{\downarrow \delta M} \tag{11}$$

$$r_{q,l'}[p'] = \left(\left(z_q[p'] e^{-j\frac{2\pi p' l'}{N}} \right) \star \Pi_N[p'] \right)_{\downarrow N_e} \tag{12}$$

By considering a noise-free and ideal channel transmission (*i.e.* $s[p'] = y[p']$), one gets:

$$r_{q,l'}[p'] = \left((s_{l'+\delta N q}[p'] \star g^*_{l'}[-p'])_{\downarrow \delta M} \star \Pi_N[p'] \right)_{\downarrow N_e} \tag{13}$$

where $s_l[p] = s[p] e^{-j\frac{2\pi p l}{\delta M N}}$. Subtituting $s[p']$ by its expression given by (7), we obtain the expression derived in (14), where the cross correlation function $R^{l'}_{l-l'}[p] = g_l[p] \star g^*_{l'}[-p] = R^0_{l-l'}[p] e^{-j\frac{2\pi p l'}{\delta M N}}$.

$\mathfrak{F}[p']_{\downarrow N_e} \triangleq \left(R^{l'}_{\delta(q-k)N}[p']_{\downarrow \delta M} \star \mathbb{H}_{l'-l+\delta(q-k)N}[p'] \right)_{\downarrow N_e}$ should be a weighted Dirac function to enable a simple one tap equalization. Therefore, $\mathfrak{F}[p']$ should have a compact support within the set $\{-N_e, ..., N_e\}$. For this purpose, it can be straightforwardly shown that $N_{\text{CP}}\delta M$ should be greater than the length of $g_l[p] \star g^*_{l'}[-p]$. Hence, the first necessary condition to enable a simple one tap equalization is the following where K is the FB overlapping factor.

$$N_{\text{CP}} > \frac{2K}{\delta} \tag{15}$$

In this case, we can rewrite (14) as:

$$r_{q,l'}[p'] = \sum_{k=0}^{M-1} \sum_{l \in \Omega} \mathfrak{F}[0] d_{k,l}[p'] e^{j\frac{2\pi p' N_e}{N}(l - l' + \delta(k-q)N)} \tag{16}$$

$$
\begin{aligned}
r_{q,l'}[p'] &= \sum_{k=0}^{M-1}\sum_{l\in\Omega}\Bigg(\Bigg(g_{l'}^{*}[-p']\star\Bigg(\left(d_{k,l}[p']_{\uparrow N_e}\star\Pi_{N_e}[p']\right)_{\uparrow\delta M}\star g_l[p']\Bigg)e^{j\frac{2\pi p'}{\delta MN}(l-l'+\delta(k-q)N)}\Bigg)\star\Pi_N[p']\Bigg)_{\downarrow N_e}\\
&= \sum_{k=0}^{M-1}\sum_{l\in\Omega}\Bigg(\Bigg(\Bigg(\underbrace{g_{l'+\delta(q-k)N}[p']\star g_{l'}^{*}[-p']}_{R^{l'}_{\delta(q-k)N}[p']}\star\\
&\qquad\qquad\Big(\left(d_{k,l}[p']_{\uparrow N_e}\star\Pi_{N_e}[p']\right)_{\uparrow\delta M}e^{j\frac{2\pi p'}{\delta MN}(l-l'+\delta(k-q)N)}\Big)\Bigg)_{\downarrow\delta M}\star\Pi_N[p']\Bigg)_{\downarrow N_e}\\
&= \sum_{k=0}^{M-1}\sum_{l\in\Omega}\left(R^{l'}_{\delta(q-k)N}[p']_{\downarrow\delta M}\star\left(d_{k,l}[p']e^{j\frac{2\pi p' N_e}{N}(l-l'+\delta(k-q)N)}\right)_{\uparrow N_e}\right)\star\\
&\qquad\qquad\left(\underbrace{\Pi_{N_e}[p']e^{j\frac{2\pi p'}{N}(l-l'+\delta(k-q)N)}\star\Pi_N[p']}_{\mathbb{H}_{l'-l+\delta(q-k)N}[p']}\right)_{\downarrow N_e}\\
&= \sum_{k=0}^{M-1}\sum_{l\in\Omega}\Bigg(\Bigg(\underbrace{R^{l'}_{\delta(q-k)N}[p']_{\downarrow\delta M}\star\mathbb{H}_{l'-l+\delta(q-k)N}[p']}_{\mathfrak{F}[p']}\Bigg)_{\downarrow N_e}\star\left(d_{k,l}[p']e^{j\frac{2\pi p' N_e}{N}(l-l'+\delta(k-q)N)}\right)\Bigg)
\end{aligned}
\tag{14}
$$

where $\mathfrak{F}[0]=0$ if $(l-l'+\delta(k-q)N)$ is not multiple of N, and otherwise it is given by:

$$
\begin{aligned}
\mathfrak{F}[0] &= \sum_{\tau=-N_{\mathrm{CP}}/2}^{N_{\mathrm{CP}}/2} R^{l'}_{\delta(q-k)N}[\delta M\tau]\\
&= \sum_{\tau=0}^{\delta M-1} G\left(\frac{l'-N\tau}{\delta MN}\right)^{*}\\
&\qquad\times G\left(\frac{l'+\delta(q-k)N-N\tau}{\delta MN}\right)
\end{aligned}
\tag{17}
$$

Consequently, we rewrite (16) as:

$$
\begin{aligned}
r_{q,l'}[p'] &= \left|G\left(\frac{l'}{\delta MN}\right)\right|^2 d_{q,l'}[p']\\
&\quad+\sum_{(k,l)\in\mathbb{Y}^{*}_{q,l'}}\Bigg[G\left(\frac{l'}{\delta MN}\right)^{*}\\
&\qquad\times G\left(\frac{l'+\delta(q-k)N}{\delta MN}\right)d_{k,l}[p']\Bigg]
\end{aligned}
\tag{18}
$$

where $\mathbb{Y}^{*}_{q,l'}=\mathbb{Y}_{q,l'}\backslash\{(q,l')\}$ and $\mathbb{Y}_{q,l'}$ is defined as $\mathbb{Y}_{q,l'} = \{(k,l)\in\{0,...,M-1\}\times\Omega\}$ with $\left(\frac{l-l'}{N}+\delta(k-q)\right)\in\mathbb{Z}$. We observe that the received signal $r_{q,l'}[p']$ is composed of two terms. The first one is related to the useful data symbol $d_{q,l'}[p']$, and the second one represents an interference term generated by the data symbols transmitted over the other subbands. However, this interference is highly attenuated thanks to the filter selectivity $G(f)$. For instance, we can show that the normalized spectral distance between the center of a subband of interest q and the nearest interfering frequency tone $l+\delta Nk$ (such that $(k,l)\in\mathbb{Y}^{*}_{q,l'}$) is $\frac{3}{2M}$ when $\delta<2/3$, whereas $G(f)\approx 0$ when $f\notin[\frac{-1}{M},\frac{1}{M}]$.

As a conclusion, FFT-FBMC can not guarantee the perfect reconstruction. Indeed, even if the proposed OFDM-based precoding avoids high energy adjacent subband interference, it can not entirely cancel ICI. However and unlike FBMC-OQAM, it is possible through a proper waveform design to intrinsically highly reject this interference (see Section III).

B. BF-OFDM waveform

Block-Filtered OFDM (BF-OFDM) is the second OFDM-precoded FBMC waveform to be studied in this paper. The main difference with respect to FFT-FBMC is the receiver scheme. Indeed, while FFT-FBMC performs the matched processing at

the receiver side, the BF-OFDM is designed to only perform a transposition in frequency without any filtering stage. The BF-OFDM receiver is thus reduced to a simple DFT like in CP-OFDM. To do so, the transmitter scheme must be slightly modified with respect to FFT-FBMC depicted in Figure 1. However, the FFT-FBMC transmitter scheme will be considered in a first time.

As for the FFT-FBMC, BF-OFDM has already been introduced and its model derived in [23] with a rate factor δ set to $1/2$. This section aims at extending the BF-OFDM model to any rate factor δ.

The sub-band allocation only depends on the frequency response of the transmitted signal and thus is the same as the one used in FFT-FBMC as it does not depend on the receiver scheme according to (10).

1) Receiver scheme

As the proposed subband allocation scheme avoids ICI with adjacent bands, it encourages the use a single DFT at the receiver side to capture at once the entire waveform symbol. The length of the corresponding transmitted signal (in samples) for N_s transmitted symbol per frequency tones can therefore be expressed as follows:

$$KM + M\delta(N_s(N + N_{\mathrm{CP}}) - 1) \tag{19}$$

Lemma 1: Applying a $MN\delta$-point DFT (same sampling frequency as the signal) at the receiver side ensures perfect reconstruction of a single-frequency-tone signal if the following expression is verified

$$N_{\mathrm{CP}} \geq \lfloor K/\delta \rfloor - 1 \tag{20}$$

The proof is given in Appendix A and the results are reminded below.
For a transmission over the frequency tone $k = l + q_0 N\delta + \frac{N\delta}{2}$ (subcarrier l of the q_0^{th} carrier), one obtains:

$$r_{q_0,l}[n] = G\left[\frac{l}{\delta MN}\right] d_{q_0,l}[n] + i_{\mathrm{ISI}k}[n] \tag{21}$$

where $r_{q_0,l}[n]$ denotes the received symbol (after the DFT) at time instant n and with $i_{\mathrm{ISI}k} = 0$ if $N_{\mathrm{CP}} \geq \lfloor K/\delta \rfloor - 1$ and otherwise (22).

Consequently, perfect reconstruction can be ensured as long as the cyclic prefix length satisfies the condition (20). Otherwise, the orthogonality property is broken and interference is generated. The interference term is composed of signal distortion induced by partial reconstruction and an ISI component. The expression obtained for BF-OFDM is highly similar to the one derived for FFT-FBMC (15) but without the factor 2. This extra factor appears for FFT-FBMC because of the filtering stage performed at the receiver side which does not exist for BF-OFDM.

Lemma 2: Perfect reconstruction can no longer be ensured for a multi-frequency-tone transmission

The expression of the corresponding received signal is given in (23). The third term corresponds to the ICI. It is generated by the precoding stage. Indeed as the OFDM modulators have a periodicity of N they generate in-band aliases and thus ICI [23]. This interference term can not be avoided which implies that perfect reconstruction can not be ensured. In other words, BF-OFDM can not be designed in order to be complex orthogonal, like the OFDM, however as it will be shown later on Near-Perfect Reconstruction (NPR) can still be ensured (also valid for FFT-FBMC). A later paragraph will be dedicated to this aspect but first we will focus on the compensation of the complex coefficient G of the useful term.

2) Filter Predistortion

By focusing on the useful term in (23), one can observe that it is affected by a coefficient related to the filter response G. It can be observed that this coefficient only depends on the subcarrier index l but not the carrier's. To properly recover the symbol, this distortion needs to be compensated. It can be done by applying the following coefficient:

$$P[l] = \frac{G^*\left[\frac{l}{\delta MN}\right]}{\left|G\left[\frac{l}{\delta MN}\right]\right|^2} \tag{24}$$

The compensation coefficient can be applied through a point-wise multiplication on all the active subcarrier signals. This coefficient only depends on the filter frequency responses G and is constant over time. Therefore, the idea is to apply a predistortion at the transmitter side instead of compensating at the receiver. This is motivated by several reasons: i) Doing so, the receiver does not need to know the filtering performed at the transmission side to properly operate and it thus satisfies the specification transparency condition [26], ii) the receiver

$$i_{\mathrm{ISI}k}[n] = -\sum_{p=N_1}^{N_1+\lfloor K/\delta \rfloor - N_{\mathrm{CP}}-2} \left(\sum_{\nu=0}^{(p-N_1+1)M\delta-1} g[\nu] a_{q_0}[p+N_{\mathrm{CP}}+n(N+N_{\mathrm{CP}})] e^{j\frac{2\pi q_0 \nu}{M}} \right) e^{-j\frac{2\pi k \nu}{MN\delta}}$$
$$+ \sum_{p=-\lfloor K/\delta \rfloor - 1}^{-N_{\mathrm{CP}}} \left(\sum_{\nu=KM+pM\delta}^{KM-1} g[\nu] a_{q_0}[p+N_{\mathrm{CP}}+(n-1)(N+N_{\mathrm{CP}})] e^{j\frac{2\pi q_0 \nu}{M}} \right) e^{-j\frac{2\pi k \nu}{MN\delta}} \quad (22)$$

$$r_{q_0,l}[n] = \sum_{p=0}^{N-1} \left(\sum_{\nu=0}^{KM-1} g[\nu] \sum_{r=0}^{M-1} a_r[p+N_{\mathrm{CP}}+n(N+N_{\mathrm{CP}})] e^{j\frac{2\pi r \nu}{M}} \right) e^{-j\frac{2\pi k(\nu+pM\delta)}{MN\delta}}$$
$$= G\left[\frac{l}{\delta MN}\right] d_{q_0,l}[n] + i_{\mathrm{ISI}k}[n] + \sum_{\substack{k'=k+\epsilon N \\ 0\le k' \le MN\delta-1}} G\left[\frac{l}{\delta MN} + \frac{\epsilon}{M\delta}\right] d_{r',k'-r'N\delta}[n] \quad (23)$$

with $r' = \lfloor k'/N\delta \rfloor$

scheme can be reduced to a simple $MN\delta$-point DFT as in OFDM, iii) it provides the possibility to have different filter shape/parametrization on the active subbands to be able to demodulate them all. Consequently, a filter-predistortion block is prepended to the precoding stage as illustrated in Figure 3.

This extra predistortion stage have no impact on the subband allocation. Indeed, even if it impacts on the transmitted spectrum (by flatening the useful band) it has no impact on the main lobe length and the periodicity of the precoding response and hence has no impact on subband allocation rule.

3) Interference Rejection

As aforementioned, two sources of interferences impact on the system: ISI generated by the overlap in time and ICI induced by the precoding scheme. By further studying the expression (23), we can notice that it is possible to fully cancel the ISI. Indeed if the CP is long enough, no portion of the previously transmitted signal is captured (see *Lemma 1*).

As enlarging the CP reduced the spectral efficiency, this condition may not be interesting for high data rate configuration. This point will be discussed in further details later on. When it comes to the ICI, it can not be prevented. Indeed, it is induced by the upsampling of subband signals performed by the filter-bank which generates in-band aliases. However, one can observe that those terms are attenuated by the filter response G. By considering well frequency localized filter shapes, it will be possible to highly reject the ICI terms. This aspect will be further studied in Section III.

4) Final Scheme

The block diagram of the transmitter and receiver schemes are depicted in Figure 3. The transmitter is composed of three distinct stages: filter pre-compensation stage, OFDM-based precoding and a PPN filter-bank. The two latter are the same as in FFT-FBMC. Each carrier of the filter-bank is fed by a CP-OFDM modulator. We have shown that if the CP length satisfies (20) the ISI is entirely cancelled. Besides, if only a part of the N available OFDM sub-carriers is allocated, it is possible to avoid ICI from adjacent filter-bank carriers. The allocation rule is the same used in FFT-FBMC (10).

The receiver is reduced to a simple DFT without any filtering. The size of the DFT is determined by the number of filter-bank carrier M, the number of precoding sub-carriers N and the rate reduction factor δ. The proposed receiver satisfies the so called specification transparency property advocated in latest RAN discussions [26]. It means that the receiver is able to operate without any knowledge about the filtering performed at the transmission side. It is even possible to fully recover signals from different transmitters using distinct prototype filters.

III. Numerology Proposals

A. LTE numerology

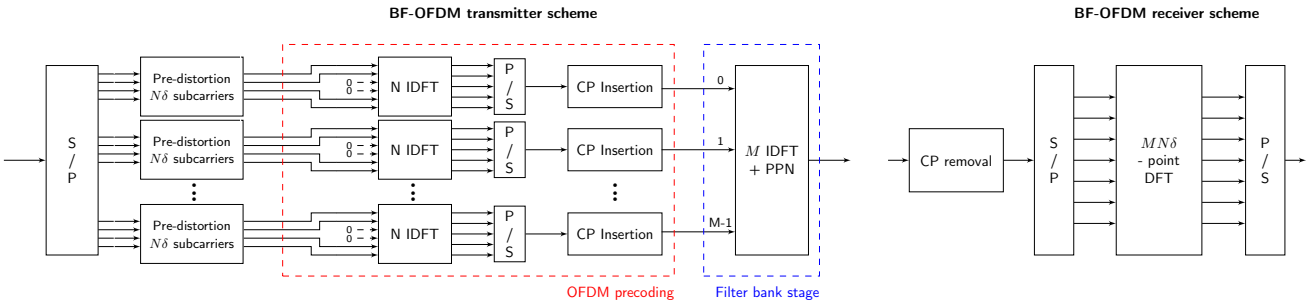

Figure 3. Block-Filtered OFDM transmitter and receiver schemes

The aim of this section is to determine the waveform configuration (*i.e.* the set of waveform parameters) to be compatible with the LTE numerology. For sake of simplicity, only the 10 MHz configuration will be addressed. Nonetheless, the same approach can be reused for other bands.

The total number of subcarriers must equal 1024 as in 10 MHz LTE which leads to the condition (25) and the sampling frequency must be set to 15.36 MHz. As a reminder, M corresponds of the number of subbands and $N\delta$ the number of subcarriers per subband. Ideally, the value of M must be maximized (and thus $N\delta$ minimized) to obtain narrow subbands and therefore an efficient filtering.

$$MN\delta = 1024 \tag{25}$$

A second condition is to satisfy the symbol density of LTE. The analytical expression of the spectral efficiency is the same for the two proposed waveforms. Assuming, N_s the number of transmitted symbols, M_a the number of active filter bank carriers, r the modulation efficiency (including both the modulation order and the coding rate), the spectral efficiency can be expressed as follows [23][27]:

$$\begin{aligned}\eta &= \frac{\delta N N_s M_a r}{KM + \delta M\left(N_s(N+N_{\mathrm{CP}})-1\right)} \\ &\xrightarrow{N_s\to\infty} r\frac{M_{\mathrm{a}}}{M}\frac{N}{N+N_{\mathrm{CP}}}\end{aligned} \tag{26}$$

As in CP-OFDM, the spectral efficiency is reduced because of the CP insertion. However, one can observe that δ has no impact on the spectral efficiency because the subband allocation has been adapted to the time structure of the signal. It implies that (27) must be satisfied so as to ensure the LTE symbol density. As N_{CP} is an integer number, the minimum value of N that still satisfies (27) is 128 (with $N_{\mathrm{CP}} = 9$).

$$\frac{N}{N+N_{\mathrm{CP}}} = \frac{1024}{1024+72} \tag{27}$$

As a consequence, if the typical rate factor $\delta = 1/2$ is considered then $M = 16$. In other words, there would be 16 subbands of 960 kHz. The subbands are therefore too wide (to be compared with a RB and thus with 180 kHz). To increase the number of subands and bring them closer to a LTE RB, lower values of the rate factor δ will be considered thanks to the analytical analysis provided in the previous section. According to Figure 2, decreasing δ helps rejecting the intrinsic interference in the frequency domain. However, it also increases the overlap in time. The interference rejection criterion will be considered as well so as to guarantee NPR for both waveforms.

However, the complexity of the transceiver (either FFT-FBMC or BF-OFDM) is expected to increase with the number of subbands. The complexity should be kept at a reasonable level because of hardware implementation and power consumption especially for battery-powered devices. Consequently, both intrinsic interference rejection and complexity will be evaluated as Key Performance Indicators (KPI) to determine the best configuration to use.

1) KPI 1: Intrinsic interference rejection

It has been observed in the previous section that for both waveforms the interference terms are attenuated by the filter response ((18) for FFT-FBMC and (23) for BF-OFDM). Therefore, a filter design based on the intrinsic interference rejection is considered. The Signal-to-Interference Ratio (SIR) is used as indicator assuming an ideal and noiseless

transmission and is evaluated by means of numerical simulations will be preferred for the study.

The optimization is performed on Gaussian filter shapes [28]. Gaussian filters are interesting as they are well localized in both time and frequency domains. The time localization helps rejecting the ISI coming from adjacent symbols in time and the frequency localization the ICI induced by in-band aliases of the signal. The trade-off between time and frequency localization is determined by the Bandwidth-Time (BT) product parameter.

2) KPI 2: Complexity

The complexity of a transceiver scheme can be evaluated by counting the number of complex multiplications required to transmit a symbol (assuming that all subbands and all subcarriers are active). The filter pre-compensation scheme applying a complex coefficients on each frequency tones and therefore requires $MN\delta$ complex multiplications (only for BF-OFDM). The precoding scheme is composed of M N-point OFDM modulators set in parallel. Assuming the Cooley-Tukey algorithm, the number of complex multiplications for a N-point FFT is thus $N/2\log_2(N)$. However in our case, only a contiguous portion of the subcarriers are used: $N\delta$ out of N. Therefore the complexity of one OFDM modulator can be reduced to $N/2\log_2(N\delta)$. The polyphase-network filter bank needs KM complex multiplications for the filtering and $M/2\log_2(M)$ for the IFFT stage per block. As a consequence, one can obtain:

$$\begin{aligned}\mathcal{C}_{\mathrm{FFT-FBMC,Tx}} &= MN/2\log_2(N\delta) \\ &\quad + N\left(M/2\log_2(M) + KM\right) \end{aligned} \tag{28}$$

$$\begin{aligned}\mathcal{C}_{\mathrm{BF-OFDM,Tx}} &= MN\delta + MN/2\log_2(N\delta) \\ &\quad + N\left(M/2\log_2(M) + KM\right) \end{aligned} \tag{29}$$

The complexity metric will also be assessed by estimating the normalized complexity with respect to the LTE-10MHz OFDM transmitter (30) and the FBMC/OQAM transmitter (31). The comparison with CP-OFDM highlights the complexity difference w.r.t to LTE systems. However, this comparison may not be relevant as the proposed waveforms are by construction different from LTE technology. The comparison with FBMC-OQAM allows a comparison with another filtered waveform based on the the filtering process. The complexity of the FBMC-OQAM transceiver results from the filtering with $K \times 1024$ multiplications ($K = 4$ will be assumed) and the 1024-point FFT. Because of the OQAM transmission, two FBMC-OQAM symbols must be transmit to transmit a complex symbol, hence the factor 2 in (31).

$$\begin{aligned}\mathcal{C}^1_{\mathrm{FFT-FBMC/BF-OFDM,Tx}} &= \frac{\mathcal{C}_{\mathrm{FFT-FBMC/BF-OFDM,Tx}}}{\mathcal{C}_{\mathrm{CP-OFDM,Tx}}} \\ &= \frac{\mathcal{C}_{\mathrm{FFT-FBMC/BF-OFDM,Tx}}}{512\log_2(1024)} \end{aligned} \tag{30}$$

$$\begin{aligned}\mathcal{C}^2_{\mathrm{FFT-FBMC/BF-OFDM,Tx}} &= \frac{\mathcal{C}_{\mathrm{FFT-FBMC/BF-OFDM,Tx}}}{\mathcal{C}_{\mathrm{FBMC/OQAM,Tx}}} \\ &= \frac{\mathcal{C}_{\mathrm{FFT-FBMC/BF-OFDM,Tx}}}{2\left(4\times 1024 + 512\log_2(1024)\right)} \end{aligned} \tag{31}$$

When it comes to the receiver complexity, thanks to the dual Tx/Rx structures of CP-OFDM, FBMC/OQAM and FFT-FBMC and by construction of BF-OFDM, the following equalities are considered:

$$\mathcal{C}_{\mathrm{CP-OFDM,Rx}} = \mathcal{C}_{\mathrm{CP-OFDM,Tx}}$$

$$\mathcal{C}_{\mathrm{FBMC/OQAM,Rx}} = \mathcal{C}_{\mathrm{FBMC/OQAM,Tx}}$$

$$\mathcal{C}_{\mathrm{FFT-FBMC,Rx}} = \mathcal{C}_{\mathrm{FFT-FBMC,Tx}}$$

$$\mathcal{C}_{\mathrm{BF-OFDM,Rx}} = \mathcal{C}_{\mathrm{CP-OFDM,Rx}}$$

As for the transmitter, we can define $\mathcal{C}^1_{\mathrm{FFT-FBMC/BF-OFDM,Rx}}$ and $\mathcal{C}^2_{\mathrm{FFT-FBMC/BF-OFDM,Rx}}$ as the normalized complexity of the receiver (either FFT-FBMC or BF-OFDM) with respect to respectively the CP-OFDM and FBMC/OQAM.

B. Application to the proposed waveforms

The filter optimisation and the complexity evaluation are summarized in Table I for FFT-FBMC and Table II for BF-OFDM. For all the configurations, $(N, N_{\mathrm{CP}}) = (128, 9)$ and $K = 4$. The 16-subband configuration corresponds to the starting configuration with 960 kHz subbands. Configurations with reduced δ are therefore studied. When δ decreases (for constant K), the achievable SIR level increases. However, the complexity significantly rises as well except for the BF-OFDM receiver scheme. The limiting indicator thus appears to be the complexity and not the near-orthogonality condition. The ideal configuration would be with $\delta = 1/32$ as a LTE RB is multiple of the subband size (*i.e.* 60 kHz). It is the only configuration that can somehow filter a

RB. However, the induced transceiver complexity is too large (about 60 times more complex than a LTE transmitter scheme) that makes it poorly appealing. An in-between configuration will be therefore preferred to benefit from a narrow subband with an acceptable complexity increase. The configuration $\delta = 1/8$ will be therefore considered for the performance evaluation.

IV. Application

Some KPIs will be evaluated for the two proposed waveforms: FFT-FBMC and BF-OFDM. For comparison, CP-OFDM and FBMC-OQAM will be used as reference for the following simulations. The conventional LTE 10 MHz broadband configurations are considered for the four waveforms as depicted in Table III.

A. Near-orthogonality property

The first KPI to be assessed is the orthogonality property of the waveform. It is done by observing the transmultiplexer response which corresponds to the spreading of constellation symbols over time and frequency domains assuming perfect propagation (ideal channel and noiseless). To do so, the received power is measured after the receiver processing when a unique symbol (real-valued with unitary energy) is transmitted at a given time $\times$ frequency position. It gives a graphical representation of the intrinsic interference induced by the modulation scheme. The results are given in Figure 4.

For CP-OFDM, the received power is concentrated at only a unique time $\times$ frequency position. It means that no interference is generated and that the waveform satisfies the strict orthogonality. When it comes to FBMC-OQAM, the power is measured before taking the real value of the received symbol (*i.e.* where the equalisation/detection stage is applied). One can observe that the real symbol is spread over adjacent positions in both time and frequency. It is due to the time and the frequency overlaps. The power of the intrinsic interference generated in FBMC/OQAM equals the power of data [7]. This intrinsic interference is cancelled at the receiver side by taking the real part of the received symbols (the interference is maintained in quadrature with the useful symbol thanks to the phase offset)[12].

The two waveforms of interest are non-orthogonal as well. Indeed, one can observe that the transmultiplexer response for both of them is not reduced

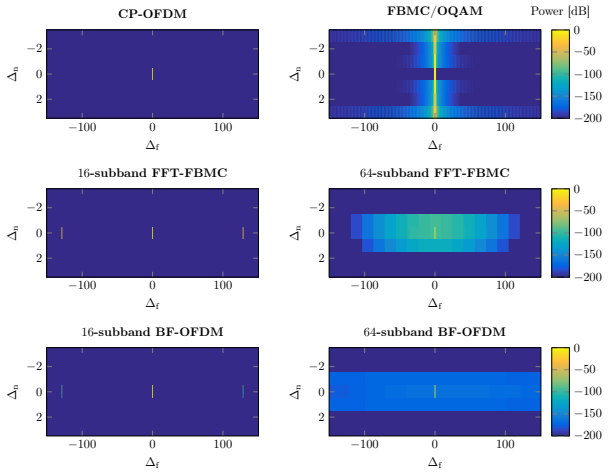

Figure 4. Transmultiplexer response of the considered waveforms where Δ_f denote the subcarrier offset and Δ_n the time instant offset.

to a single point as in CP-OFDM. However, unlike FBMC-OQAM, the intrinsic interference spread much less power (higher SIR level) For the two 16-subband configurations, there is no intrinsic interference generated in time as the value of δ $(1/2)$ is high enough. Only interference in the frequency domain is generated. Indeed, one can observe ICI every N (128) subcarriers. For the 64-subband configurations, the value of delta is reduced and therefore the considered CP length, 9, is not high enough to prevent ISI in time. That is why intrinsic interference is generated over time according to (15) and (20). Regarding the ICI, intrinsic interference is spread over the whole band with BF-OFDM because of the FFT-based receiver scheme while it is contained in a subband with FFT-FBMC thanks to its subband processing. Although the two waveforms provides similar SIR level, the intrinsic interference distributions are different mainly because of the receiver scheme.

B. Spectral Confinement

The frequency localization of the considered waveforms are assessed in this section. The Power Spectral Density (PSD) of the four waveforms are given in Figure 5. One can observe that CP-OFDM emits the highest OOB emissions because of its rectangular pulse. On the other hand, FBMC-OQAM provides the most confined spectrum thanks to its subcarrier wise filtering. FFT-FBMC and BF-OFDM offer performance in between. The spectral confinement is relaxed with respect to FBMC-OQAM as the filtering is performed over a subband instead of 15-kHz band. Nonetheless, the spectral

Table I
OPTIMISATION RESULTS FOR FFT-FBMC.

Rate factor δ	1/2	1/4	1/8	1/16	1/32
Number of subbands M	16	32	64	128	256
Subband Size [kHz]	960	480	240	120	60
Maximum SIR level [dB] (BT)	81 (0.28)	90 (0.61)	94 (1.26)	95 (2.55)	95 (5.12)
$\mathcal{C}^1_{\mathrm{FFT-FBMC,Tx}}$	3.6	7.2	14.4	28.8	57.6
$\mathcal{C}^2_{\mathrm{FFT-FBMC,Tx}}$	1	2	4	8	16
$\mathcal{C}^1_{\mathrm{FFT-FBMC,Rx}}$	3.6	7.2	14.4	28.8	57.6
$\mathcal{C}^2_{\mathrm{FFT-FBMC,Rx}}$	1	2	4	8	16

Table II
OPTIMISATION RESULTS FOR BF-OFDM.

Rate factor δ	1/2	1/4	1/8	1/16	1/32
Number of subbands M	16	32	64	128	256
Subband Size [kHz]	960	480	240	120	60
Maximum SIR level [dB] (BT)	90 (0.27)	135 (0.52)	145 (1.08)	148 (2.2)	150 (4.45)
$\mathcal{C}^1_{\mathrm{BF-OFDM,Tx}}$	3.8	7.4	14.6	29	57.8
$\mathcal{C}^2_{\mathrm{BF-OFDM,Tx}}$	1.056	2.056	4.056	8.056	16.056
$\mathcal{C}^1_{\mathrm{BF-OFDM,Rx}}$	1	1	1	1	1
$\mathcal{C}^2_{\mathrm{BF-OFDM,Rx}}$	0.28	0.28	.28	0.27	0.28

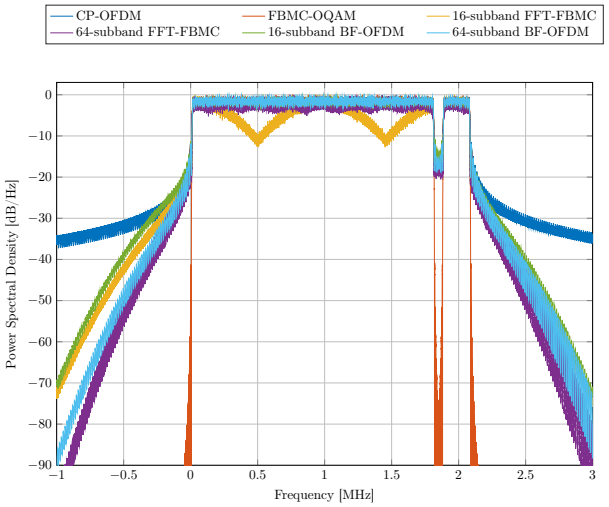

Figure 5. PSD of the considered waveforms for a 10-RB and 1-RB frequency allocations spaced by a 90 kHz guard band.

confinement is improved with respect to CP-OFDM and the side lobe rejection is slightly improved with the 64-subband configurations. However, the near-OOB spectrum (*i.e.* just adjacent to the allocated band) is still composed of high side lobes as we can observe in the spectrum hole (90 kHz wide). Besides, one can observe the main difference between the FFT-FBMC and BF-OFDM spectra. Indeed, the distinct subbands can be easily distinguished with FFT-FBMC (especially with the 16-subband configuration) while the BF-OFDM in-band spectrum is flat thanks to its pre-distortion stage.

C. Channel Performance

The Bit Error Rate (BER) will now be evaluated over LTE channels models. Two multi-path channel models with rayleigh distributed coefficients are considered for this study: a short delay channel (EPA) with 5 Hz maximum Doppler shift (Jake's model) and a long delay spread channel (ETU) with 300 Hz maximum Doppler shift (Jake's model)[29]. For this study, uncoded systems are considered so as to emphasize the impact of the intrinsic interference on the performance. Besides, the channel is assumed to be perfectly known at the receiver side (perfect CSI) so as to provide a fair comparison between the considered waveforms as in FBMC-OQAM the

Table III
WAVEFORM CONFIGURATIONS.

	OFDM		FBMC-OQAM	
Number Carriers N	1024		Number Carriers N	1024
CP Length	72		Overlapping Factor K	4
			Prototype Filter	Phydyas

	FFT-FBMC		BF-OFDM	
	16 subbands	64 subbands	16 subbands	64 subbands
Number FB Carriers M	16	64	16	64
Number OFDM Subcarriers N	128	128	128	128
δ	0.5	0.125	0.5	0.125
CP Length	9	9	9	9
Prototype Filter	Gaussian $\alpha = 0.28$	Gaussian $\alpha = 1.26$	Gaussian $\alpha = 0.27$	Gaussian $\alpha = 1.08$

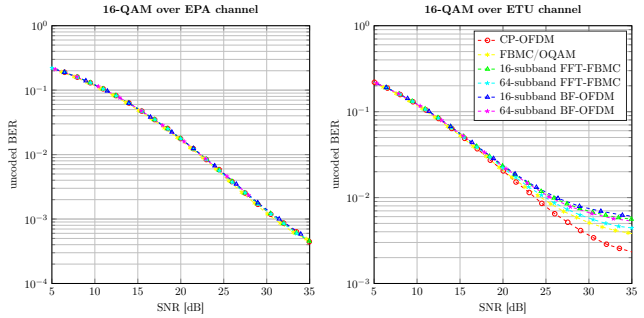

Figure 6. Uncoded BER for SISO 16-QAM over 5-Hz EPA and 300-Hz ETU channels.

channel estimation process is different [30][31]. Zero-Forcing is used for the equalisation stage. MIMO performances are not evaluated in this study. However, the performance with the 2×1 Alamouti scheme applied to FFT-FBMC has been addressed in [22].

The performance results are depicted in Figure 6. One can observe that for short delay spread (EPA) there is no performance penalty. However when the channel delay spread is high (ETU), both FFT-FBMC and BF-OFDM exhibit an error floor earlier than CP-OFDM and FBMC-OQAM. Indeed the two waveforms suffer from high ISI induced by the symbol overlap in time. However, the performance penalty is reduced with the 64 subband configurations.

D. Asynchronous multi-user uplink

The asynchronous multi-user uplink is one typical 5G scenario where the interference induced by relaxing the synchronization in time between active users is evaluated. For this scenario, two users are considered. The user of interest has a 3-RB allocation and is adjacent to a 9-RB asynchronous user (without any guard band between the two users). The level of distortion is assessed at the subcarrier level for different timing offsets (from minus half CP-OFDM symbol duration to plus half symbol duration). Observing the interference at the subcartier level allows to determine the guard band required to satisfy a target worst distortion level. The results are depicted in Figure 7.

CP-OFDM provides the worst performance. The subcarriers just adjacent to the interfering user are highly impacted with MSE greater than -15 dB. Then the Mean Square Error (MSE) slightly decreases while moving away from the interfering user. It is induced by the high sides lobes and slow decay rate of the cardinal sine frequency response of the OFDM. The subcarrier-wise filtering performed by the FBMC/OQAM allows an excellent user isolation as long as a guard band of at least 15 kHz (*i.e.* one subcarrier) spaces the two users. For FFT-FBMC and BF-OFDM, users are placed in adjacent subbands. The subcarriers near the interfering users are significantly impacted by the asynchronous user as in OFDM. However, FFT-FBMC provides a

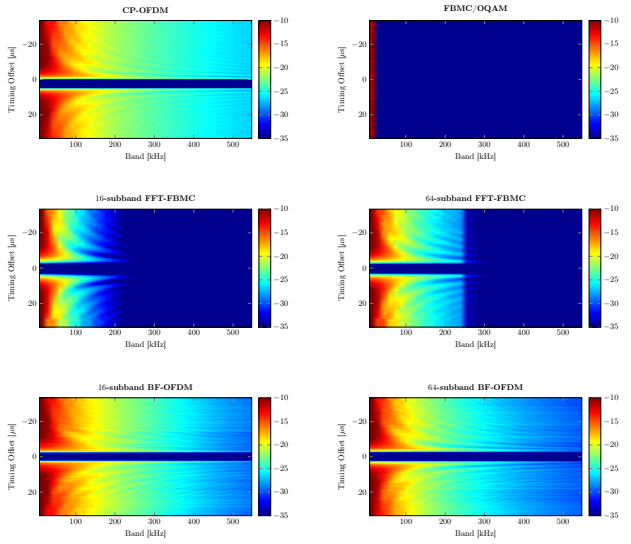

Figure 7. Asynchronous scenario results for a 9-RB interfering user and a 3-RB user of interest without any guard band between the two users.

strong subband isolation. The configuration with 64 subbands demonstrates slightly worst performance but 4 times more subbands are supported. For BF-OFDM, the MSE decreases with the guard band better than for OFDM. As a consequence, supporting non orthogonal subbands transmission can be efficiently achieved when both side lobe rejection and receive filtering techniques are considered.

V. Conclusion

In this paper, the OFDM-based precoding for filter-bank waveforms has been studied as an alternative to the OQAM signaling. Two waveforms relying on the proposed precoding scheme have been introduced namely FFT-FBMC and BF-OFDM. Strong intrinsic interference rejection can be provided for a LTE configuration which makes the proposed waveforms near complex orthogonal. Therefore, interference cancellation techniques are not necessary at the receiver which allows a straightforward reuse of communication techniques such as Space Time Block Coding and LTE-like channel estimation. However, the filtering is relaxed with respect to FBMC/OQAM and is now applied at the subband level. The number of multiplexed subbands can be increased by lowering the rate factor. A strong robustness against short delay channels is achieved. However, a slight performance penalty with respect to legacy OFDM occurs for long delay spread channels induced by the time structure of the signal. The main interest of filtered waveforms lies in the transmission of non-orthogonal subbands as for instance the asynchronous multi-user uplink scenarios. The proposed waveforms exhibit improved user isolation, even significant for the FFT-FBMC, in the aforementioned evaluation scenario which allows a better bandwidth use for such scenarios. The proposed solutions are thus appealing for multiplexing non orthogonal signals. In addition to that, a straightforward deployment can be provided by the BF-OFDM as it relies on a simple LTE-receiver. The change of waveform is thus completely transparent for a LTE UE. And significant performance gains, in terms of subband isolation, can be achieved by considering the filter-bank based receiver and thus the FFT-FBMC scheme.

The proposed study focuses on intrinsic interference rejection and shows that NPR can be ensured. Nonetheless, the induced complexity of the proposed precoding scheme prevents an efficient implementation. Besides, the proposed prototype filter design method may limit the obtained performance for the considered scenarios. As a consequence, lowering the precoding complexity and designing the prototype filter on side lobe rejection may be interesting to study as perspective.

Appendix A
Proof of Lemma 1

This appendix aims at giving the proof of lemma 1 by establishing the circularity condition for BF-OFDM.

One transmitted waveform symbol (either FFT-FBMC or BF-OFDM) is composed of $N + N_{\mathrm{CP}}$ FB symbols (of length KM) denoted from now as blocks. The N_{CP} first blocks correspond to the CP (redundancy) and the N last to the useful symbol. It seems worth reminding that consecutive waveform symbol overlap in time.

The $MN\delta$-point DFT is synchronized with the beginning of the useful symbol. By using the linearity of the Fourier transform function, it is possible to apply the Fourier Transform on each captured blocks. There are three categories of blocks: 1) those which are entirely captured in one piece, 2) the blocks transmitted before for whom only the tail is received and 3) the last ones for whom only the beginning is captured.

We can determine N_1 the number of blocks of category 1):

$$KM + (N_1 - 1)M\delta \leq MN\delta \tag{A.1}$$

which leads to:

$$N_1 = N - \left\lfloor \frac{K}{\delta} \right\rfloor + 1 \tag{A.2}$$

When it comes to the second group:

$$N_2 = \min(\lfloor K/\delta \rfloor - 1, N_{\mathrm{CP}}) \tag{A.3}$$

It is assumed that the time shift $M\delta$ divides the length of one block KM and therefore $\frac{K}{\delta} \in \mathbb{Z}$.

In a first time, it is assumed that only one waveform symbol is transmitted and only FB-carrier q_0 is used. For sake of clarity, the time istant indices n are omitted in a first time. Applying the DFT on the received signal is equivalent to apply it on each block and sum all the outputs which gives:

$$\begin{aligned}
r_k &= \sum_{\nu}^{MN\delta-1} s[\nu + MN_{\mathrm{CP}}\delta] e^{-j\frac{2\pi}{MN\delta}k\nu} \\
&= \sum_{p=0}^{N_1-1} \left(\sum_{\nu=0}^{KM-1} g[\nu] a_{q_0}[p + N_{\mathrm{CP}}] e^{j\frac{2\pi q_0 \nu}{M}} \right) e^{-j\frac{2\pi k\nu}{MN\delta}} \\
&+ \sum_{p=-N_2}^{-1} \left(\sum_{\nu=KM+lM\delta}^{KM-1} g[\nu] a_{q_0}[p + N_{\mathrm{CP}}] e^{j\frac{2\pi q_0 \nu}{M}} \right) e^{-j\frac{2\pi k\nu}{MN\delta}} \\
&+ \sum_{p=N_1}^{N-1} \left(\sum_{\nu=0}^{(p-N_1+1)M\delta-1} g[\nu] a_{q_0}[p + N_{\mathrm{CP}}] e^{j\frac{2\pi q_0 \nu}{M}} \right) e^{-j\frac{2\pi k\nu}{MN\delta}} \\
r_k &= \sum_{p=0}^{N_1-1} \left(\sum_{\nu=0}^{KM-1} g[\nu] a_{q_0}[p + N_{\mathrm{CP}}] e^{j\frac{2\pi q_0 \nu}{M}} \right) e^{-j\frac{2\pi k\nu}{MN\delta}} \\
&+ \sum_{\substack{p'=N-1 \\ p'=p+N}}^{N-N_2} \left(\sum_{\nu=(l'-N_1)M\delta}^{KM-1} g[\nu] a_{q_0}[p' + N_{\mathrm{CP}}] e^{j\frac{2\pi q_0 \nu}{M}} \right) e^{-j\frac{2\pi k\nu}{MN\delta}} \\
&+ \sum_{p=N_1}^{N-1} \left(\sum_{\nu=0}^{(l-N_1+1)M\delta-1} g[\nu] a_{q_0}[p + N_{\mathrm{CP}}] e^{j\frac{2\pi q_0 \nu}{M}} \right) e^{-j\frac{2\pi k\nu}{MN\delta}}
\end{aligned} \tag{A.4}$$

Perfect reconstruction can thus be ensured if $N - N_2 = N_1$ leading to $N_2 = \lfloor N/\delta \rfloor - 1$ implying that

$$N_{\mathrm{CP}} \geq \lfloor K/\delta \rfloor - 1 \tag{A.5}$$

As a consequence

$$r_k = \sum_{p=0}^{N-1} \left(\sum_{\nu=0}^{KM-1} g[\nu] a_{q_0}[p + N_{\mathrm{CP}}] e^{j\frac{2\pi q_0 \nu}{M}} \right) e^{-j\frac{2\pi k\nu}{MN\delta}} \tag{A.6}$$

otherwise

$$\begin{aligned}
r_k &= \sum_{p=0}^{N_1-1} \left(\sum_{\nu=0}^{KM-1} g[\nu] a_{q_0}[p + N_{\mathrm{CP}}] e^{j\frac{2\pi q_0 \nu}{M}} \right) e^{-j\frac{2\pi k\nu}{MN\delta}} \\
&+ \sum_{p=N_1}^{B_1} \left(\sum_{\nu=0}^{(p-N_1+1)M\delta-1} g[\nu] a_{q_0}[p + N_{\mathrm{CP}}] e^{j\frac{2\pi q_0 \nu}{M}} \right) \\
&\quad \times e^{-j\frac{2\pi k\nu}{MN\delta}} \\
&+ \sum_{p=B_2}^{N-1} \left(\sum_{\nu=0}^{KM-1} g[\nu] a_{q_0}[p + N_{\mathrm{CP}}] e^{j\frac{2\pi q_0 \nu}{M}} \right) e^{-j\frac{2\pi k\nu}{MN\delta}}
\end{aligned} \tag{A.7}$$

with $B_1 = N_1 + \lfloor K/\delta \rfloor - N_{\mathrm{CP}} - 2$ and $B_2 = N_1 + \lfloor K/\delta \rfloor - N_{\mathrm{CP}} - 1$.

For a transmission tone $k = l + q_0 N\delta + \frac{N\delta}{2}$, for l satisfying subband allocation (10) and G defined as for (8), one obtains:

$$r_{q_0,l} = G \left[\frac{l}{\delta MN} \right] d_{q_0,l} + i_{\mathrm{ISI}k} \tag{A.8}$$

with $i_{\mathrm{ISI}k}[n]$ given in (A.9). When only one waveform is sent, the orthogonality can be broken (apparition of ISI terms) if the CP is not long enough.

If more waveform symbols are considered:

$$\begin{aligned}
r_k[n] = &\sum_{\nu=0}^{MN\delta-1} s[\nu + MN_{\mathrm{CP}}\delta + n(N + N_{\mathrm{CP}})M\delta] \\
&\times e^{-j\frac{2\pi}{MN\delta}k\nu}
\end{aligned} \tag{A.10}$$

From results given in Step 1, one can obtain that for a transmission tone $k = l + q_0 M\delta + \frac{N\delta}{2}$:

$$r_{q_0,l}[n] = G \left[\frac{l}{\delta MN} \right] d_{q_0,l}[n] + i_{\mathrm{ISI}k}[n] \tag{A.11}$$

with $i_{\mathrm{ISI}k}[n] = 0$ if $N_{\mathrm{CP}} \geq \lfloor K/\delta \rfloor - 1$ and otherwise (A.12). By considered a shortened CP, there is therefore a double effect compromising the perfect reconstruction: i) the circularity is broken and ii) samples from previously transmitted symbol are received.

$$i_{\mathrm{ISI}k} = \begin{cases} 0 & \text{if } N_{\mathrm{CP}} \geq \lfloor N/\delta \rfloor - 1 \\ -\sum_{p=N_1}^{N_1+\lfloor K/\delta \rfloor - N_{\mathrm{CP}}-2} \left(\sum_{\nu=0}^{(p-N_1+1)M\delta-1} g[\nu] a_{q_0}[p+N_{\mathrm{CP}}] e^{j\frac{2\pi q_0 \nu}{M}} \right) e^{-j\frac{2\pi k\nu}{MN\delta}} & \text{otherwise} \end{cases} \tag{A.9}$$

$$\begin{aligned} i_{\mathrm{ISI}k}[n] = &- \sum_{p=N_1}^{N_1+\lfloor K/\delta \rfloor - N_{\mathrm{CP}}-2} \left(\sum_{\nu=0}^{(p-N_1+1)M\delta-1} g[\nu] a_{q_0}[p+N_{\mathrm{CP}}+n(N+N_{\mathrm{CP}})] e^{j\frac{2\pi q_0 \nu}{M}} \right) e^{-j\frac{2\pi k\nu}{MN\delta}} \\ &+ \sum_{p=-\lfloor K/\delta \rfloor - 1}^{-N_{\mathrm{CP}}} \left(\sum_{\nu=KM+pM\delta}^{KM-1} g[\nu] a_{q_0}[p+N_{\mathrm{CP}}+(n-1)(N+N_{\mathrm{CP}})] e^{j\frac{2\pi q_0 \nu}{M}} \right) e^{-j\frac{2\pi k\nu}{MN\delta}} \end{aligned} \tag{A.12}$$

REFERENCES

[1] Next Generation Mobile Network Alliance, "5G White Paper," *online*, Feb. 2015.

[2] H. Shariatmadari, R. Ratasuk, S. Iraji, A. Laya, T. Taleb, R. Jäntti, and A. Ghosh, "Machine-type communications: current status and future perspectives toward 5G systems," *IEEE Communications Magazine*, vol. 53, no. 9, pp. 10–17, September 2015.

[3] "View on 5G Archicture," 5GPPP Architecture Working Group, July 2016.

[4] B. Farhang-Boroujeny, "OFDM Versus Filter Bank Multicarrier," *IEEE Signal Processing Magazine*, vol. 28, no. 3, pp. 92–112, May 2011.

[5] M. Bellanger and J. Daguet, "TDM-FDM Transmultiplexer: Digital Polyphase and FFT," *IEEE Transactions on Communications*, vol. 22, no. 9, pp. 1199–1205, September 1974.

[6] B. Hirosaki, "An Orthogonally Multiplexed QAM System Using the Discrete Fourier Transform," *IEEE Transactions on Communications*, vol. 29, no. 7, pp. 982–989, July 1981.

[7] M. Bellanger, "FBMC physical layer: a primer," ICT-PHYDYAS Project, Tech. Rep., 2010, available on http://www.ict-phydyas.org.

[8] R. Balian, "Un principe d'incertitude fort en théorie du signal ou en mécanique quantique," *Comptes rendus de l'Académie des sciences Série II*, vol. 292, no. 20, pp. 1357–1362, 1981.

[9] J. J. Benedetto, C. Heil, and D. F. Walnut, "Differentiation and the Balian-Low Theorem," *Journal of Fourier Analysis and Applications*, vol. 1, no. 4, pp. 355–402, 1994.

[10] R. W. Chang, "Synthesis of band-limited orthogonal signals for multichannel data transmission," *The Bell System Technical Journal*, vol. 45, no. 10, pp. 1775–1796, December 1966.

[11] B. Saltzberg, "Performance of an efficient parallel data transmission system," *IEEE Transactions on Communication Technology*, vol. 15, no. 6, pp. 805–811, December 1967.

[12] P. Siohan, C. Siclet, and N. Lacaille, "Analysis and design of OFDM/OQAM systems based on filterbank theory," *IEEE Transactions on Signal Processing*, vol. 50, no. 5, pp. 1170–1183, May 2002.

[13] R. Zakaria, D. L. Ruyet, and M. Bellanger, "Maximum likelihood detection in spatial multiplexing with FBMC," in *Proc. European Wireless Conference (EW)*, Lucca, Italy, April 2010, pp. 1038–1041.

[14] H. Lin, C. Lele, and P. Siohan, "A pseudo alamouti transceiver design for OFDM/OQAM modulation with cyclic prefix," in *Proc. IEEE on Signal Processing Advances in Wireless Communications (SPAWC)*, Perugia, Italy, june 2009, pp. 300–304.

[15] M. Renfors, T. Ihalainen, and T. H. Stitz, "A block-Alamouti scheme for filter bank based multicarrier transmission," in *Proc. European Wireless Conference (EW)*, Lucca, Italy, april 2010, pp. 1031–1037.

[16] V. Vakilian, T. Wild, F. Schaich, S. ten Brink, and J. F. Frigon, "Universal-filtered multi-carrier technique for wireless systems beyond LTE," in *Proc. IEEE Global Communications Conference (Globecom)*, Atlanta, USA, december 2013, pp. 223–228.

[17] X. Zhang, M. Jia, L. Chen, J. Ma, and J. Qiu, "Filtered-OFDM - Enabler for Flexible Waveform in the 5th Generation Cellular Networks," in *Proc. IEEE Global Communications Conference (GLOBECOM)*, San Diego USA, Dec 2015, pp. 1–6.

[18] R. Zayani, Y. Medjahdi, H. Shaiek, and D. Roviras, "WOLA-OFDM: a potential candidate for asynchronous 5G," in *Proc. IEEE Global Communications Conference (Globecom)*, Washington, USA, december 2016, pp. 1–5.

[19] C. Lélé, P. Siohan, and R. Legouable, "The Alamouti Scheme with CDMA-OFDM/OQAM," *EURASIP Journal on Advanced Signal Processing*, vol. 2010, Jan. 2010.

[20] R. Nissel, J. Blumenstein, and M. Rupp, "Block frequency spreading: A method for low-complexity MIMO in FBMC-OQAM," in *Proc. IEEE International Workshop on Signal Processing Advances in Wireless Communications (SPAWC)*, Sapporo, Japan, July 2017, pp. 1–5.

[21] R. Zakaria and D. Le Ruyet, "A novel FBMC scheme for Spatial Multiplexing with Maximum Likelihood detection," in *Proc. IEEE International Symposium on Wireless Communication Systems (ISWCS)*, York, UK, September 2010, pp. 461–465.

[22] ——, "A Novel Filter-Bank Multicarrier Scheme to Mitigate the Intrinsic Interference: Application to MIMO Systems," *IEEE Transactions on Wireless Communications*, vol. 11, no. 3, pp. 1112–1123, March 2012.

[23] D. Demmer, R. Gerzaguet, J. Doré, D. Le Ruyet, and D. Kténas, "Block-Filtered OFDM: a novel waveform for future wireless technologies," in *Proc. IEEE International Conference on Communications (ICC)*, Paris, France, May 2017.

[24] R. Gerzaguet, D. Demmer, J. Doré, and D. Kténas, "Block-Filtered OFDM: a new promising waveform for multi-service scenarios," in *Proc. IEEE International Conference on Communications (ICC)*, Paris, France, May 2017.

[25] R. Zakaria and D. L. Ruyet, "Theoretical Analysis of the Power

Spectral Density for FFT-FBMC Signals," *IEEE Communications Letters*, vol. 20, no. 9, pp. 1748–1751, September 2016.

[26] "Technical Specification Group Radio Acces Network - Study on New Radio (NR) Access Technology: Physical Layer Aspects," 3GPP TR 38.802, V2.0.0, Release 14, March 2017.

[27] Y. Medjahdi, S. Traverso, R. Gerzaguet, H. Shaiek, R. Zayani, D. Demmer, R. Zakaria, J. Doré, M. Mabrouk, D. L. Ruyet, Y. Loüet, and D. Roviras, "On the road to 5G: Comparative study of Physical layer in MTC context," *IEEE Access*, vol. 5, pp. 26 556–26 581, 2017.

[28] A. Sahin, I. Guvenc, and H. Arslan, "A Survey on Multicarrier Communications: Prototype Filters, Lattice Structures, and Implementation Aspects," *IEEE Communications Surveys Tutorials*, vol. 16, no. 3, pp. 1312–1338, Third 2014.

[29] 3GPP, "LTE; Evolved Universal Terrestrial Radio Access (E-UTRA); Base Station (BS) radio transmission and reception. TS 36.104 v.8.13.0 Release 8," 3GPP, Tech. Rep., 07-2012.

[30] E. Kofidis, "Channel estimation in filter bank-based multicarrier systems: Challenges and solutions," in *Proc. International Symposium on Communications, Control and Signal Processing (ISCCSP)*, Athens, Greece, May 2014, pp. 453–456.

[31] J. Doré, V. Berg, and D. Kténas, "Channel estimation techniques for 5G cellular networks: FBMC and multiuser asynchronous fragmented spectrum scenario," *Transactions on Emerging Telecommunications Technologies*, vol. 26, no. 1, pp. 15–30.